AIAA JOURNAL
Vol. 38, No. 10, October 2000

Short-Scale Instabilities in Trailing Wake Vortices in a Stratified Fluid

Donald P. Delisi* and Robert E. Robins†
NorthWest Research Associates, Inc., Bellevue, Washington 98009-3027

Measurements of the evolution of wingtip trailing wake vortices in nonturbulent and unsheared density-stratified fluids are reported, using both laboratory experiments and a three-dimensional numerical code. As is widely known, and as our laboratory and numerical results confirm, the primary instability for these vortices in an unstratified fluid is the Crow instability, which has a characteristic initial wavelength of around $8.6b_0$, where b_0 is the initial separation distance between the vortices. In stratified fluids, however, our laboratory observations and numerical simulations show an instability with a shorter wavelength of around b_0–$2b_0$. This instability appears at a time in the evolution when the vertical migration of the vortices has reached nearly its maximum extent. The observed instability grows both in amplitude and wavelength with time. When the vortex Froude number is around one, the instability first becomes visible at a nondimensional time T of around 2 and reaches a maximum at T of around 4. For a commercial aircraft, the latter time corresponds to distances of around 10–25 km behind the aircraft. In flight, at $T \sim 4$, the vertical peak-to-peak amplitude oscillation of the vortex cores due to this instability could be up to 20 m with a horizontal wavelength around 100 m.

Nomenclature

b_0	= initial distance between the vortices
Fr	= Froude number, V_0/Nb_0
g	= gravitational acceleration
H	= nondimensional descent distance, h/b_0
h	= dimensional descent distance
m	= axial wavenumber of a perturbation
N	= Brunt–Väsäilä frequency of stratified fluid, $N^2 = -(g/\rho_0)\,\mathrm{d}\rho/\mathrm{d}z$
r_0	= radius of the vortex cores
T	= nondimensional time, tV_0/b_0
t	= dimensional time
V_0	= initial descent speed of the vortices
x	= axial coordinate
y	= cross-axial coordinate
z	= vertical coordinate
Γ	= vortex circulation, $2\pi V_0 b_0$
ε	= measure of numerical accuracy
ν	= kinematic viscosity
$\rho(z)$	= ambient density profile
ρ_0	= representative value of ambient density

I. Introduction

A LIFTING wing generates counter-rotating wake vortices that generally roll up downstream of the wing into a single pair of vortices. As this pair of vortices descends in an unstratified fluid, the vortex cores become unstable, and a periodic oscillation develops. As the oscillation amplitude increases, the distance between the cores increases at some locations, while the cores approach each other at other locations. When the cores touch each other (commonly called linking or reconnection), vortex rings are formed. This sinusoidal instability that develops in the initially two-dimensional line vortex pair, first reported by Scorer[1] and first analyzed by Crow,[2] is commonly called the Crow instability. Crow's analysis was performed for vortices in a nonturbulent, unstratified, fluid and showed that the initial instability has a wavelength of $8.6b_0$, where b_0 is the initial separation distance between the vortices. Crow's predictions have been verified both in the laboratory[3] and with three-dimensional numerical codes.[4]

Recently, several laboratory studies in unstratified fluids have reported on the evolution of vortex core instabilities with wavelengths substantially smaller than $8.6b_0$. In unstratified water experiments, Thomas and Auerbach[5] observed the evolution of vortices generated by the rotation and stopping of a single flat plate. In these experiments, long-scale waves, with wavelengths similar to the Crow wavelength, and shorter-scale waves, with wavelengths of order b_0 or less, were observed only on the stopping vortex. Experiments with only a single vortex showed no instabilities. In related, also unstratified, water experiments, Leweke and Williamson[6,7] observed short-scale and long-scale instabilities in a counter-rotating vortex pair generated by the motion of two flat plates. Their experiments look qualitatively similar to those of Thomas and Auerbach,[5] except that the instabilities developed on both vortices, probably because the vortices in Leweke and Williamson[6,7] were generated simultaneously. Finally, the measurements of Sarpkaya and Suthon[8] on vortex pairs in an unstratified fluid approaching a free surface strongly suggest that short-scale instabilities are responsible for some of the various surface phenomena they observed.

In stratified flows, vortex evolution is different than in unstratified flows. In high-resolution, two-dimensional numerical simulations, Spalart[9] reported that the vortices propagated farther in a stratified fluid than in an unstratified fluid. However, in three-dimensional laboratory experiments[3] and three-dimensional numerical simulations,[10] stratification was shown to inhibit the vertical migration of the vortices, and they propagated less far than in an unstratified fluid. None of these experiments or simulations reported on short-scale (wavelength b_0–$2b_0$) instabilities developing on the vortex cores.

Recently, we have examined the three-dimensional behavior of wake vortices from model wings in density-stratified fluids without turbulence and shear, and we have observed instabilities of a much shorter scale than the Crow instability. Our instabilities initially appear earlier in the evolution of the vortices than in the above studies[5–7] and only in stratified flows. In this paper, we report on both laboratory observations and numerical simulations of these instabilities. We discuss the experimental facility in Sec. II and the numerical code in Sec. III. Results are presented in Sec. IV, Sec. V contains a discussion of these results, and conclusions are presented in Sec. VI.

II. Experimental Facility

Our laboratory experiments were performed in a water-filled towing tank measuring 9.8 m long, 0.9 m wide, and 1.0 m deep. For

Presented as Paper 97-1784 at the AIAA 28th Fluid Dynamics Conference, Snowmass, CO, 29 June–2 July 1997; received 15 September 1998; revision received 15 March 2000; accepted for publication 23 March 2000.

*Senior Research Scientist, P.O. Box 3027; Don@NWRA.com. Senior Member AIAA.

†Research Scientist, P.O. Box 3027; Bob@NWRA.com. Senior Member AIAA.

Table 1 Summary of runs used in this study

Run number	Tow speed, cm/s	Angle of attack, deg	Trailing edge depth, cm	N, s^{-1}	Fr
6383	212.9	6.0	16.33	0	∞
6387	248.3	6.0	16.33	0	∞
6392	248.7	6.0	17.46	0.41	1.10
6393	251.0	6.0	17.46	0.41	1.10
6395	160.9	6.0	17.15	0.42	0.73
6396	300.5	3.0	16.99	0.42	1.00

these experiments, the water depth was 0.9 m. To generate wake vortices, a single wing was towed down the tank at a constant depth below the surface. The depth of the wing in the water was always greater than six chords to ensure that the wing was in the linear part of the stratification profile and to minimize the effect of the free surface. The wing consisted of a rectangular plate that was curved in a smooth, circular, arc with a camber of 12.1%. The plate was 0.081 cm thick and had a span of 10.52 cm and a chord of 2.42 cm. The aspect ratio, the square of the wing span divided by the wing area, was 4.3. A thin strut of 0.16 cm thickness and 1.27 cm width was connected to the centerline of the wing. The strut was attached to a carriage that rode above the tank and was towed by steel cables. The towing speed used for these measurements ranged from 160 to 300 cm/s, giving chord Reynolds numbers ranging from 3.9×10^4 to 7.3×10^4 (compared to aircraft chord Reynolds numbers on the order of tens of millions). The angle of attack of the wing (relative to a zero angle of attack when the leading and trailing edges were horizontal) was 6 deg (3 deg for run 6396; see Table 1). The leading edge of the wing was up, so the vortices generated from the wing migrated down toward the bottom of the tank. The coefficient of lift for this wing was 0.87 at 6 deg and 0.50 at 3 deg.

Flow visualization was performed primarily using fluorescein dye. Before a run, water was taken from the tank at the same depth as the wing. This water was mixed with a small amount of dye to form a dye solution that had nearly the same density as the undyed water at the depth of the wing. The dye mixture was introduced into the tank in a concentrated cloud just upstream of the test section. The dye was injected into the water just before the passage of the wing with a hypodermic syringe, with the tip located at the depth of the wing. As the wing passed through the dye cloud, dye was entrained into the cores, and this dye traveled in the same direction as the wing into the test section. In the test section, the dye was illuminated by a Spectra-Physics 5-W argon ion laser. The motion of the dye was documented on videotape using two video camcorders located at the side and the top of the tank. Grids in the test section for both the side and overhead views were recorded on the videotapes to allow the determination of length scales.

The dye appeared to have a minimal effect on either the stratification or the motion of the vortices. When injected, the dye normally stayed at the same level as the injection point and spread slowly and laminarly. In those rare cases when the dye did not stay at the injection level (these cases always occurred in an unstratified tank), the movement was always traced to slow convective currents in the tank. In those cases, no runs were performed. Several cases were performed with no dye or with smaller amounts of dye to determine the effects of the dye on the vortex motion. With no dye, either shadowgraph (for stratified cases) or particles on the bottom floor of the tank (for unstratified cases) was used to record the motion or migration speed of the vortices. In all cases, the results with the dye were identical to the results without dye to within experimental measurement error.

The tank was either unstratified using fresh water or stratified using salt water. A standard two-tank stratification method, similar to that used by Fortuin,[11] Delisi and Dunkerton,[12] and others, was used to produce linear stratification profiles. These profiles were measured using calibrated conductivity probes.

Observations using videotapes from the camcorders on the side of the tank yielded the depth of the vortex cores with time. From these measurements, we could estimate the initial vertical velocity V_0 of the vortex system, as well as the time history of the depth of the cores and the evolution of wave instabilities on the cores. Observations of the videotapes from the camcorders on the top of the tank gave the separation of the vortex cores with time, from which we could estimate the initial separation b_0 of the vortex cores.

The vortex Reynolds number is defined as Γ/ν, where Γ is the vortex circulation, defined as $2\pi V_0 b_0$, and ν is kinematic viscosity. In this study, the vortex Reynolds number ranged from 1.9×10^4 to 2.7×10^4, with only run 6395 being below 2.2×10^4. The median vortex Reynolds number in our experiments was 2.45×10^4 (compared to aircraft vortex Reynolds numbers on the order of tens of millions).

The stratification profile is used to estimate the Brunt–Väsäilä frequency N given by $N^2 = -(g/\rho_0)\, d\rho/dz$, where g is the acceleration due to gravity, ρ is density, ρ_0 is a representative density, and z is the vertical coordinate. In these experiments, N was zero (unstratified), 0.41, or 0.42 s^{-1}. The nondimensional vortex Froude number is defined as $Fr = V_0/Nb_0$. In this study, Fr ranged from 0.73 to infinite (no stratification).

A summary of the runs in this study is given in Table 1.

III. Numerical Approach

The code we used in the present study solves the primitive, Boussinesq, three-dimensional Navier–Stokes equations for an incompressible fluid. Described in detail in Refs. 4 and 10, the code uses a two-phase time stepping scheme, where the first phase evolves the flow using the second-order Adams–Bashforth method, and the second phase, sometimes called a projection phase, maintains incompressibility. The side wall boundary conditions are periodic so that fast Fourier transforms can be used to compute horizontal derivatives. For simplicity, the top and bottom boundary conditions are open (normal derivatives equal zero), and a sixth-order compact scheme, similar to one described by Lele,[13] is used to compute vertical derivatives. The two-thirds rule is used to avoid aliasing. Fourier and compact low-pass filters, in the horizontal and vertical directions, respectively, are used to control the build-up of small-scale energy. The compact filter is also based on a scheme described by Lele.[13]

The calculations of trailing vortex evolution, discussed in the next section, are initialized by a superposition of counter-rotating vortex pairs. The horizontal coordinate aligned with the axes of the vortices is denoted by x, the horizontal cross-axial coordinate by y, and the vertical coordinate by z. Initially, the axes of each component of the superposition of vortex pairs lie in the same horizontal plane and are slightly perturbed from being parallel straight lines separated by b_0. The perturbations are sinusoidal, with each sinusoid having horizontal peak-to-peak amplitude equal to 10% of b_0. The axial wavenumber m of each component pair (where m is the same for each member of the pair) typically varies from 2 to 40 in an axial domain of length $10b_0$. The axial phase of each vortex in the superposition is randomly assigned. Thus, although the vortices in each component counter-rotating pair have the same amplitude and wavenumber, they have different axial phases. As a result of the randomness of the phases, the horizontal oscillation of the axis of each composite vortex has a peak-to-peak amplitude approximately equal to 4% of b_0 (in contrast to 10% of b_0 for each component vortex), implying that the initial separation between the composite vortices varies between 0.96 and 1.04 times b_0. The circulations for the different components vary as $m^{-5/6}$ (thus energies vary as $m^{-5/3}$), and the initial total circulation of the superposition is chosen equal to the initial total circulation of the vortices that are being simulated. In planes perpendicular to the x-coordinate, the vortex components have circular Gaussian vorticity distributions. The cores of the vortex components are defined by the core radius r_0, where r_0 is the value at which the vorticity falls to $1/e$ of its peak value. In these simulations, r_0 was $0.16b_0$ (16% cores). The migration direction of the vortices is downward, for easy comparison with the vortices produced in the laboratory.

Four calculations were performed for this study as summarized in Table 2. Computer system batch queue constraints for time and memory affected the choice of parameters. It is worth noting that there were five points across the vortex core diameters for the lower (F1r, N0r) resolution calculations and nine points for the higher (F1R, N0R) resolution calculations. The vortex Reynolds number,

Table 2 Calculations performed in this study

Case	Domain size,[a] b_0	Grid[a]	ΔT, $\Delta t V_0/b_0$	Fr
F1r	$10\times5\times7$	$256\times64\times91$	0.00202	1
F1R	$10\times5\times5$	$512\times128\times129$	0.00111	1
N0r	$20\times5\times8$	$512\times64\times103$	0.00202	∞
N0R	$10\times5\times7$	$512\times128\times181$	0.00121	∞

[a]For domain size and grid, the order is axial × cross-axial × vertical.

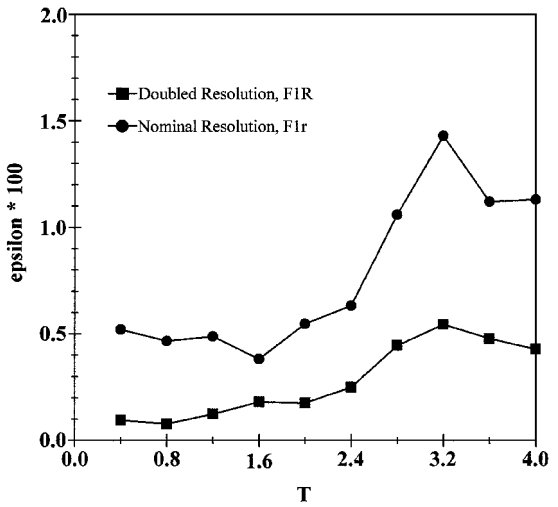

Fig. 1 Incompressibility criterion ε vs nondimensional time T.

Γ/ν, for all calculations was 1465, a number empirically determined to yield better agreement with laboratory results than higher or lower values.

To assess the credibility of the calculations, we monitored the quantity $\varepsilon = \sqrt{(\langle \mathrm{DIV}^2\rangle/\langle \mathrm{GRADSQ}\rangle)}$, where

$$\mathrm{DIV} = \frac{\partial u}{\partial x} + \frac{\partial v}{\partial y} + \frac{\partial w}{\partial z}$$

$$\mathrm{GRADSQ} = \left(\frac{\partial u}{\partial x}\right)^2 + \left(\frac{\partial v}{\partial y}\right)^2 + \left(\frac{\partial w}{\partial z}\right)^2$$

where $\langle\ \rangle$ indicates an average over the computational domain. The quantity ε is a measure of the incompressibility of computed flows; the value of ε for an incompressible flow should be zero. Our criterion for a calculation to be of acceptable accuracy was that the value of ε at the conclusion of the calculation be less than 0.01.

Figure 1 shows ε vs T for calculations F1r and F1R, where $T = tV_0/b_0$, and t is dimensional time. It is evident, according to the above criterion, that calculation F1r is barely acceptable for $T \gtrsim 3$, whereas calculation F1R falls well within the criterion for acceptability. Further assessment of the validity of the calculations is shown in the next section.

IV. Results

Figure 2 shows a video image from a laboratory experiment in an unstratified fluid (run 6387). This figure shows a side view of the towing tank, where the wing passed through the test section near the top of the tank, traveling from left to right in the image. The initial wing depth is shown as the dashed line near the top of the tank. The vortex cores, made visible with dye, are shown at a time of 7.0 s after the passage of the wing. (The clock is in the lower-right-hand corner and reads in tenths of a second.) The dye cloud can be seen on the left-hand side of the image. In this image, the cores are at a nondimensional depth, $H = h/b_0$, of around 3, where h is dimensional depth, and the image was taken at a nondimensional time T of around 3. The vortices in the image are undergoing Crow instability and are at a stage when the vortex cores are about to reconnect and form vortex rings. In this figure, the cores have descended most rapidly in the dye cloud on the left-hand edge of the picture and near the right edge of the picture (shown by the arrows in Fig. 2). These are the regions where the vortex cores have come closer together. The more rapid descent of these regions relative to the descent of the cores in the center of the image is a result of the closer vortex spacing at these two locations. In this image, we estimate the wavelength of the instability to be around $8.5b_0$, close to the most unstable wavelength predicted by Crow.[2] Of particular note in this figure are the dominance of the Crow instability wavelength and the absence of shorter wavelengths.

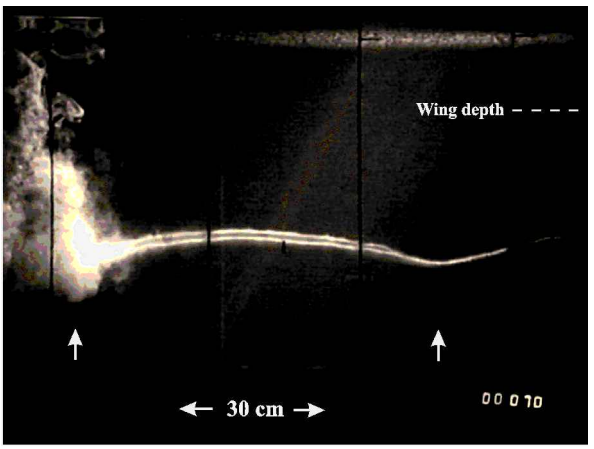

Fig. 2 Video image showing the side view of an unstratified run (run 6387) at a time of 7.0 s after passage of a wing. The wing passed from left to right in the image at a depth near the top of the image (shown by the dashed line). Dye is shown in the vortex cores, and a dye cloud can be seen on the left-hand side of the image. The vortices are about to undergo linking as the vortex lines evolve into vortex rings. Arrows show the locations where linking of the vortex cores occurs at a time slightly later than shown in the figure. Note the absence of wavelengths shorter than the Crow instability wavelength.

Figure 3 shows images from a nominally identical run at the same time after passage of the wing, except the water in this experiment is linearly stratified. In this run (run 6393), the Brunt–Väsäilä frequency, N, was 0.41 s^{-1}, and the Froude number was 1.10. Figure 3a shows a side view of the towing tank, similar to the view in Fig. 2. The time of this image is 7.0 s after passage of the wing, similar to the time in Fig. 2. In this image, we do not see the longer Crow wavelength that dominated the flow in Fig. 2. Instead, shorter-scale wavelengths are evident, particularly in the right-hand side of the image where the vortex cores are most visible (shown by the arrows). Note also that the oscillations of the vortex cores appear to be out of phase, i.e., at axial positions where one vortex moves upwards, the other vortex moves downward. This out-of-phase motion was also reported by Leweke and Williamson.[7] Figure 3b shows another view of the same run at the same time after passage of the wing. For this view, a camcorder was placed both above and to the side of the tank to give a three-dimensional perspective. In Fig. 3b, the shorter-scale wavelengths are easier to see than in Fig. 3a.

Note in Fig. 2 that the vortex system has migrated farther down into the tank than in Fig. 3a at the same time. This reduced migration distance with stratification is consistent with previous laboratory measurements of vortex migration in stratified flows.[3] Figure 4 shows vortex migration as a function of nondimensional depth vs nondimensional time for the runs in Table 1 and for the data in Sarpkaya.[3] Here, the + and × symbols represent laboratory data from two unstratified runs and the closed, shaded symbols represent laboratory data from four stratified runs. The open squares are from Sarpkaya. The dashed line is the inviscid result $H = T$. We note the following in Fig. 4. First, data from the two unstratified runs (runs 6383 and 6387) follow each other closely. This shows small run-to-run variability. (For the unstratified cases, the depth of the vortex system was evaluated away from the areas of reconnection since, after reconnection, the pinched regions rebound to near the level of the rest of the ring.) Second, the data from the two stratified runs that were performed under similar conditions (runs 6392 and 6393) also follow each other closely, again showing small run-to-run

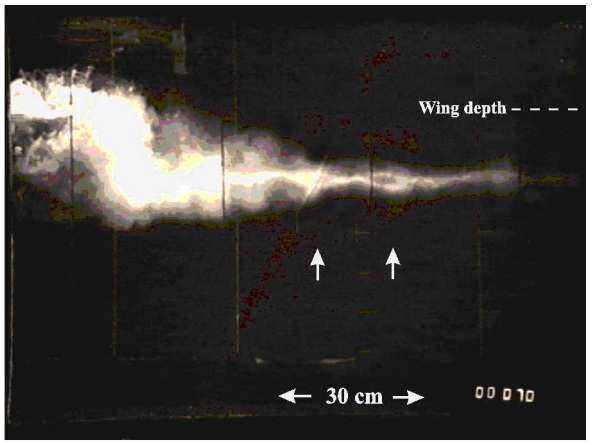

a)

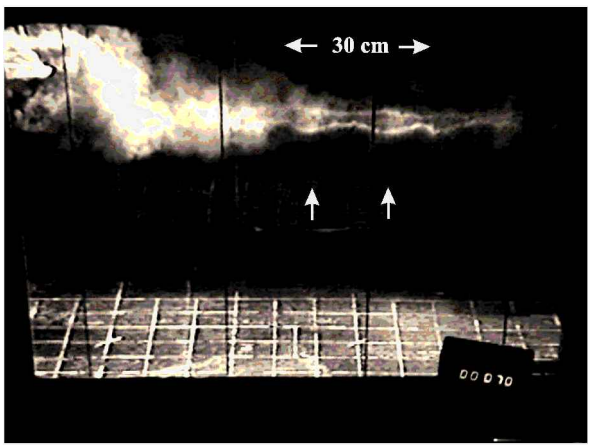

b)

Fig. 3 Same as Fig. 2 except for a stratified run (run 6393): a) side view and b) three-dimensional view. In both views, arrows point to the short-scale waves.

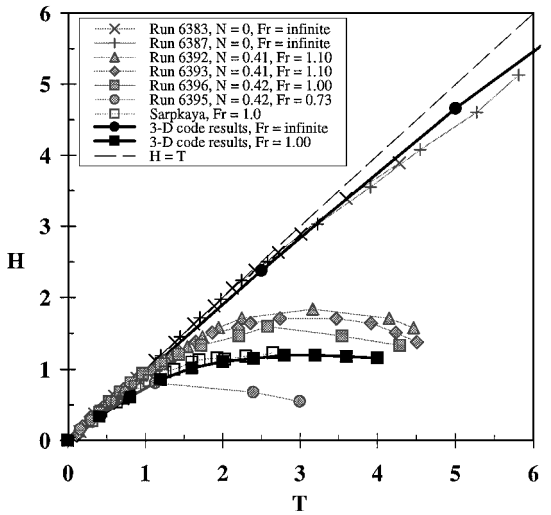

Fig. 4 Nondimensional vertical vortex migration distance vs nondimensional time for laboratory and numerical experiments for stratified and unstratified runs.

variability. (For the stratified runs, the average depth of the cores is plotted.) The other two stratified runs were performed at differing speeds and angles of attack. Regardless, all of the laboratory data in Fig. 4 are consistent in that decreasing Fr implies a smaller vortex migration in the vertical direction. Finally, we note that the nondimensional time of the images in Fig. 3 ($T \sim 3$) corresponds to near the time of the maximum migration (maximum H) for Run 6393.

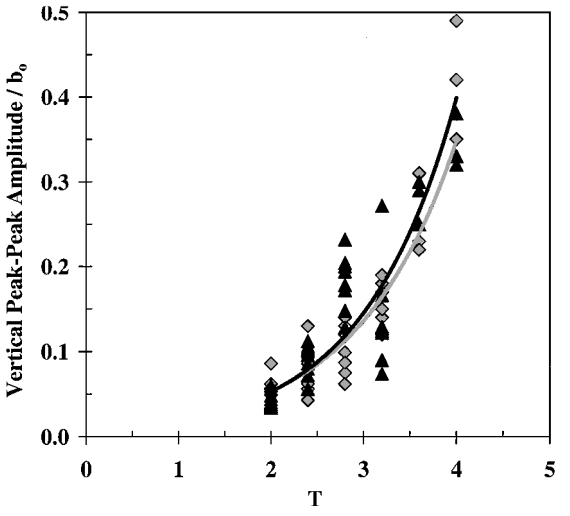

Fig. 5a Vertical peak-to-peak amplitude vs time for the low-resolution numerical results (diamonds) and the high-resolution numerical results (triangles) for the stratified cases F1r and F1R. The solid lines are exponential fits to the data.

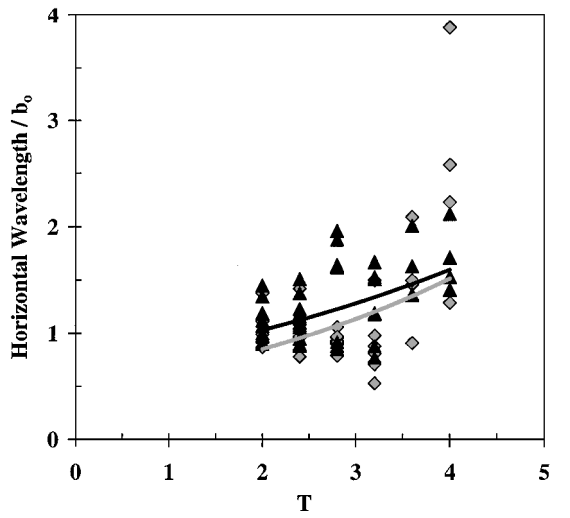

Fig. 5b Horizontal wavelength vs time for the low-resolution numerical results (diamonds) and the high-resolution numerical results (triangles) for the stratified cases F1r and F1R. The solid lines are exponential fits to the data.

Figure 5 shows growth of vertical amplitude (Fig. 5a) and horizontal wavelength (Fig. 5b) for the numerical calculations F1r and F1R. This figure shows that the results for these two calculations agree reasonably well. Because the numerical accuracy of the higher resolution calculation is at least a factor of two better than the numerical accuracy of the lower resolution calculation (Fig. 1) and the results of the two calculations agree (Fig. 5), we infer that the higher resolution calculations are accurate simulations of the phenomena under study.

Figure 4 includes results from numerical simulations for the conditions associated with Figs. 2 and 3. In Fig. 4, the solid, black symbols connected by the thick, solid lines show migration depths vs time for the high-resolution numerical simulations. The unstratified simulation, shown by the black circles and the thick, solid line, compares very well with the laboratory data. The simulation for $Fr = 1$, shown by the black squares and the thick, solid line, falls between our laboratory data for $Fr = 0.73$ and 1.0, and falls nearly on top of Sarpakaya's $Fr = 1.0$ data. We attempt to explain some of this difference with the $Fr = 1.0$ runs below. We note that ΔH, the difference in values of H between the numerical simulation and our laboratory data for $Fr = 1.0$, is around 0.3 at $T = 3$.

Figure 6 shows surface contours of vorticity from the higher resolution numerical simulation for $Fr = 1$ at times of $T = 2.4$, 3.2, and

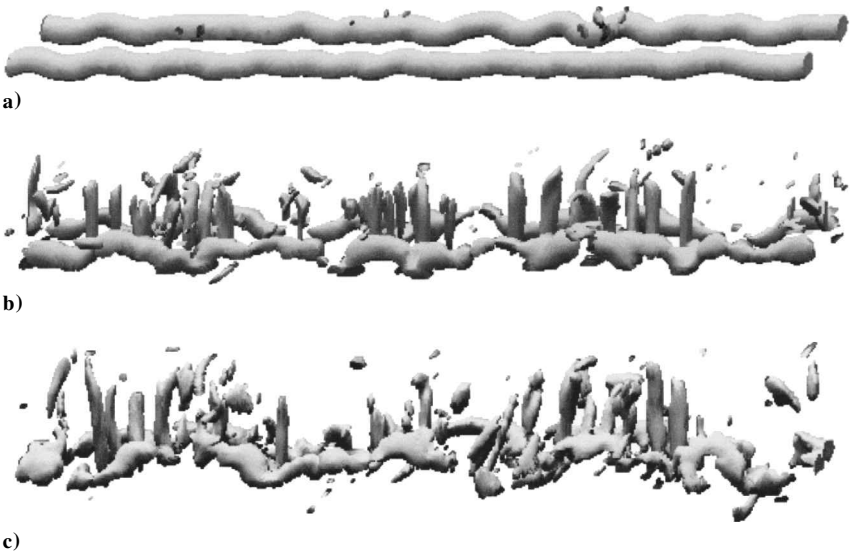

Fig. 6 Computed surface contours of vorticity from the high-resolution numerical simulation for $Fr = 1$ at nondimensional times of a) $T = 2.4$, b) $T = 3.2$, and c) $T = 4.0$.

4.0. For this simulation, the initial perturbation wavelength spectrum ranged from $5b_0$ to $0.25b_0$. The minimum resolved wavelength, determined by the resolution of the computational grid, was $0.039b_0$. This figure shows that both the amplitudes and wavelengths of the short scales predicted by the calculation grow with time. Note also that the oscillations of the vortices tend to be out of phase in the same way as we observed for the vortices in Fig. 3a.

A comparison of the observed and computed vertical component of short-scale amplitude growth with time is shown in Fig. 7. In this figure, measurements from the three laboratory runs with Froude number near unity are shown as squares, and the results from the high-resolution numerical calculation for $Fr = 1$ are shown as triangles. Numerical results for $N = 0$ are shown as circles. Multiple values at a given time show the range of amplitudes of the short scales obtained from the measurements and the calculations. An exponential fit to the stratified lab measurements is shown as a thick, solid line, and an exponential fit to the corresponding code results is shown as a thin, solid line. A very thin, solid line is the exponential fit to the numerical results for the unstratified case.

Figure 7 shows that amplitudes from both the laboratory observations and the numerical simulation for $Fr = 1$ increase with time and that the magnitude of the measured and calculated amplitudes are similar. We note that the exponential fits to the laboratory and numerical results nearly overlay. The amplitudes for the numerical $N = 0$ case are non-zero, but are more than an order of magnitude smaller than for the $Fr = 1$ case at larger times.

In Fig. 7 at a time of $T \sim 3$, the peak-to-peak amplitude of the short-scale waves for the $Fr = 1$ case ranges from around $0.1b_0$ to $0.3b_0$. These values are close to ΔH, the size of the differences we noted in Fig. 4 between the vertical migration results for the code and our laboratory measurements at $T \sim 3$. Thus, the differences we saw in Fig. 4 between our laboratory results for $Fr = 1.0$, the laboratory results for $Fr = 1.0$ from Sarpkaya, and our numerical simulation for $Fr = 1.0$ may be due, in part, to the difficulty in determining the "average" depth of the vortex system in the presence of the short-scale waves.

Figure 8 shows the horizontal wavelengths of the short scales with time. Again, the laboratory measurements are the squares, and the results from the numerical simulation for $Fr = 1$ are the triangles. The exponential fits are also shown. This figure shows that the wavelengths from both the laboratory flow and the calculation have a tendency to increase with time, and that the wavelengths range between $0.5b_0$ and $2b_0$. Note that this wavelength is significantly smaller than the Crow instability wavelength. Also shown in Fig. 8 are the wavelengths for the $N = 0$ case, and it is clear that these wavelengths grow very slowly with time.

Figure 9 shows the vertical component of the short-scale waves vs horizontal wavelength. The data symbols are the same as those used in Figs. 7 and 8. For the stratified lab measurements and stratified code simulation, the amplitudes grow with increasing wavelength. Again, for the unstratified code simulation, the amplitude stays small and relatively constant with time.

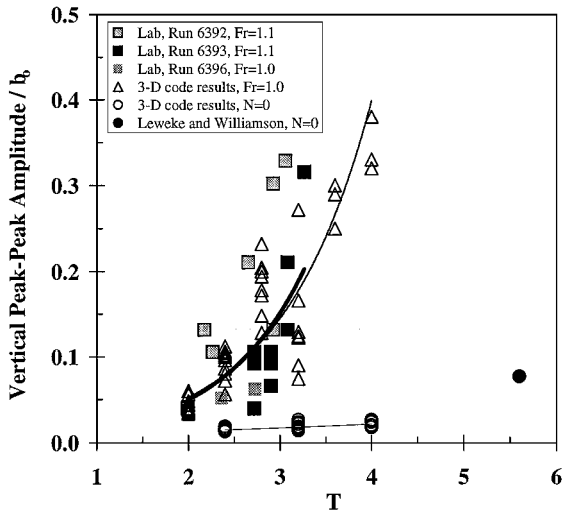

Fig. 7 Comparison of laboratory measurements and high-resolution numerical results for the vertical amplitude of the short-scale waves vs nondimensional time. Stratified laboratory data are shown by the squares; an exponential fit to have data is shown by the thick, solid line. High-resolution numerical results for the stratified case are shown by triangles; an exponential fit to these data is shown by the thin, solid line. Results for an unstratified, high-resolution numerical simulation are shown by the circles, and an exponential fit to these unstratified results is shown by the very thin, solid line. The filled circle is data from Fig. 4 in Leweke and Williamson[7] for an unstratified fluid.

V. Discussion

Table 3 shows a comparison of parameters for this study and the studies of Crow,[2] Thomas and Auerbach,[5] and Leweke and Williamson.[7] Note that all of these studies, except ours, were for unstratified flow.

Estimates of the most likely observable scales to be expected from the axial instability of a pair of trailing vortices were presented in the studies of Crow[2] and Widnall et al.[14] and the review of Widnall.[15] Crow's analysis indicated that, for a pair of vortices with core radii in the range $0.10b_0$–$0.25b_0$, the maximum amplification of axial perturbations should occur at wavelengths on the order of $8b_0$ and b_0. The former result is better known because it helps to explain

Table 3 Comparison of parameters for selected studies

Author	Type of study	Fluid	Predicted or observed horizontal wavelength	Vertical amplitude (peak-to-peak)	Observation or prediction	Times of predictions or observations, T	Vortex Reynolds number	Vortex generation mechanism	Includes axial velocity ?
Crow[2]	Analytical	Unstratified	$8.6b_0$, $\sim b_0$	Infinitesimal	Prediction	Infinitesimal	N/A[a]	N/A	No
Leweke and Williamson[7]	Analytical	Unstratified	$\sim 0.5b_0$–b_0 for short scale waves	Infinitesimal	Prediction	Infinitesimal	N/A	N/A	No
Thomas and Auerbach[5]	Laboratory experiments	Unstratified	$0.4b_0$–$0.9b_0$ (from their Table 1)	Not discussed	Observed on stopping vortex only	4.3, 5.0	(2×10^3)–(1.2×10^4)	Rotation and stopping of single flat plate	No
Leweke and Williamson[7]	Laboratory experiments	Unstratified	$0.9b_0$ for short scale waves (from their Fig. 4)	$0.2b_0$ for short scale waves (from their Fig. 4)	Observation	4.8 to 8.6	(2.4×10^3)–(2.8×10^3)	Rotation and stopping of two flat plates	No
This study	Laboratory experiments and numerical simulations	Unstratified	Observed $\sim 8.5b_0$ (Crow); $< 0.1b_0$ for short scales	Numerically predicted $< 0.03b_0$ for short scale waves	Observation and prediction	2 to 4	$\sim 2.5 \times 10^4$	Wing at angle of attack	Yes
This study	Laboratory experiments and numerical simulations	Stratified ($Fr \sim 1$)	$0.5b_0$–$2b_0$ for short scale waves	Up to $0.4b_0$ for short scale waves	Observation and prediction	2 to 4	$\sim 2.5 \times 10^4$	Wing at angle of attack	Yes

[a]N/A, Not applicable.

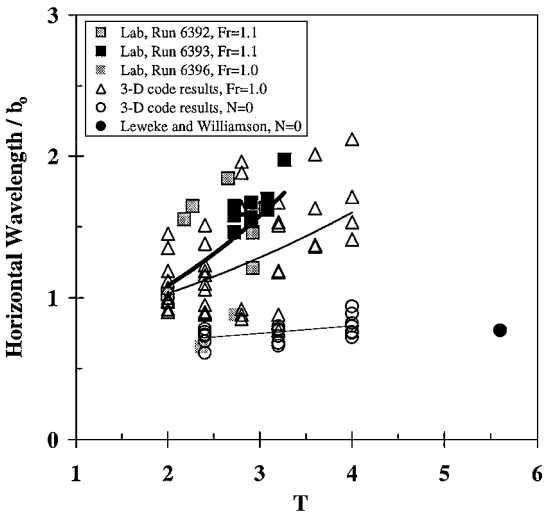

Fig. 8 Similar to Fig. 7 except for horizontal wavelength vs nondimensional time.

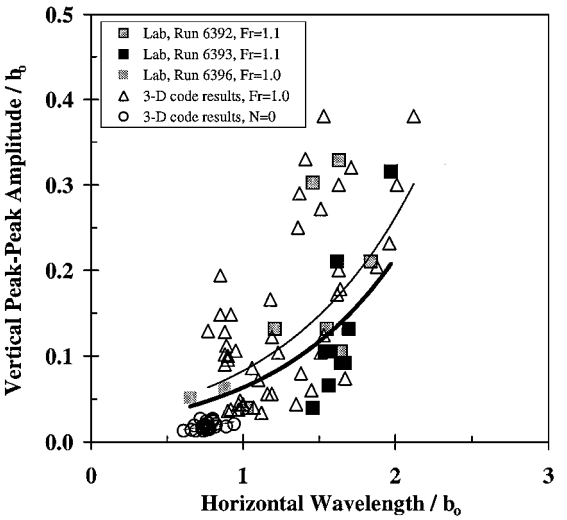

Fig. 9 Similar to Fig. 7 except for vertical amplitude vs horizontal wavelength. The data from Leweke and Williamson[7] are not shown because the nondimensional time of their observation is larger than the times of these observations.

the observed behavior of aircraft contrails. According to Crow, the larger scale is favored in the atmosphere because it is reasonably similar to the scales of naturally occurring turbulence.

As pointed out by Widnall et al.,[16] Crow's analysis is not valid for short wavelengths. However, Leweke and Williamson[7] have recently presented results, based on the work of Tsai and Widnall,[17] which are valid for short wavelengths. Their Fig. 15 shows that the maximum amplification of axial perturbations for Gaussian vortices having core radii in the range of $0.10b_0$–$0.25b_0$ will occur at wavelengths in the range $0.5b_0$–$1.0b_0$, which is similar to the range of initial wavelengths seen in our laboratory and simulation results.

We note that these results are all for vortex instability in an unstratified fluid. Our results for an unstratified fluid, shown in Fig. 2, also support the growth of wavelengths around $8b_0$ in an unstratified flow. Our stratified flow results, shown in Figs. 3, 5, 6, 8, and 9, however, show the growth of smaller-scale wavelengths of order $0.5b_0$–$3b_0$. Whereas these wavelengths are similar to the wavelength predictions of Crow[2] and Leweke and Williamson,[7] their predictions are only for unstratified flow, while we observe these short-scale waves only in stratified flow. This difference between predictions and observations in unstratified flow and observations in stratified flow is an important aspect of this paper.

It is also important to note that the results of Crow[2] and Leweke and Williamson[7] are based on linear perturbation (infinitesimal time) analyses of the kinematic relationship between vorticity and velocity in an incompressible, unstratified fluid. It is, thus, not clear to what extent these previous studies are valid for the long-time, nonlinear evolution of trailing vortices in stratified fluids, discussed here. These earlier studies do, however, provide a guide to what scales may be expected (cf. Table 3).

Comparing previous short-scale wave observations with our results, we note that Fig. 4 in Thomas and Auerbach[5] shows very small-amplitude short waves at a dimensional time, t, of 0.8 s,

larger-amplitude short waves at $t = 1.3$ s, and even larger amplitude short waves at $t = 1.7$ s. Unfortunately, we cannot determine the nondimensional times of these observations without knowledge of the rotation rate of the plate generator in this figure. Figure 4 in Ref. 7 shows short-scale waves at $T = 5.6$ and 6.8. We have analyzed the data from Fig. 4 at $T = 5.6$ and have plotted the results as the black, filled, circle in Figs. 7 and 8. We see in these figures that the $N = 0$ data point from Leweke and Williamson is reasonably consistent with our three-dimensional code results for $N = 0$. (We note that the data from Leweke and Williamson in our Fig. 7 show, strictly speaking, the horizontal peak-to-peak amplitude, as opposed to the vertical amplitude for our data. However, Fig. 6 in Leweke and Williamson shows that the instability is aligned at 45 deg to the horizontal, thus making the horizontal and vertical excursions equal.) What stands out from the comparisons in Figs. 7 and 8 is that both our laboratory and numerical results show more rapid growth and longer wavelengths of short-scale waves in stratified flows than is or has been observed in nonstratified flows. Looking at the data in both Refs. 5 and 7, we see that, even for large amplitude waves, the observed short-scale wavelength is always less than b_0. This result is unlike our observations of wavelengths of order $2b_0$ (Fig. 8). We currently do not understand the mechanism for either the more rapid growth or the longer wavelengths, but, clearly, stratification must play an important role.

Another interesting question is why the short-scale waves, observed in the nonstratified experiments of Thomas and Auerbach[5] and Leweke and Williamson,[6,7] were not observed in our own nonstratified laboratory experiments. One clue, perhaps, is in the vortex Reynolds number (see Table 3). In Thomas and Auerbach,[5] the vortex Reynolds number ranged from 2×10^3 to 1.2×10^4. In Leweke and Williamson,[6,7] the vortex Reynolds number was between 2.4×10^3 and 2.8×10^3. The lower end of these vortex Reynolds numbers imply a laminar flow, which is consistent with the photographs in these two papers. In our laboratory experiments, the median Reynolds number was 2.45×10^4, and the cell surrounding the vortex cores was clearly turbulent (as judged by rapid dye dispersion). Thus, it may be that the previous experiments observed a laminar instability that does not appear in our experiments with larger vortex Reynolds numbers and turbulence in the vortex cell surrounding the vortex cores. If, in a stratified flow, the vortex cell becomes laminar as the vertical migration of the vortex pair ceases and the vortex Reynolds number decreases, then laminar instability may also explain why we observe small-scale growth late in the evolution of the stratified vortex pair.

Another difference between our laboratory results and previous laboratory measurements is axial flow. In our experiments, axial flows are generated as the wing is towed down the tank. In the experiments of Thomas and Auerbach[5] and Leweke and Williamson,[6,7] no axial flows are generated, at least initially, since there is no axial movement of the vortex generator. However, in our numerical simulations, no initial axial flows are present either. Thus, the role of axial flow in the instability is unclear at this time.

Leweke and Williamson[7] attribute the appearance of short-scale waves in their experiments to an elliptic instability. A recent theoretical study by Billant et al.[18] supports this explanation. Since our experiments were performed with larger vortex Reynolds numbers, axial flow, and stratification, it is unclear whether we are observing the same instability as Leweke and Williamson or not. To complicate matters further, our previous numerical simulations[10] showed that stratification amplifies the rate at which Crow instability and linking occur. The role of stratification may be to dampen the turbulence in the vortex cell, thus allowing a laminar instability to grow, and/or it may be that stratification introduces small scales in the vortex cores which then amplify sooner than in an unstratified fluid. Alternately, stratification may play another, as yet undefined, role. In any case, due to the similarity of scales between our observed small scales and those of Leweke and Williamson, the elliptic instability must be suspected of playing some role in our experiments.

Another important question is whether our observations and simulations of short-scale instability is a low Reynolds number phenomenon only, or whether our results are also relevant to high Reynolds number aircraft vortices. Previously, we have shown good agreement between the migration and vortex decay of our laboratory vortices and aircraft vortex measurements,[19] where the aircraft measurements were obtained under the Aircraft Vortex Spacing System (AVOSS) Program[20] conducted by NASA. Additional, encouraging comparisons we have obtained will be presented in the near future. Based on these comparisons, we suspect that our low-Reynolds-number results are at least indicative of the results we would see at much higher Reynolds numbers. Future work in this area should concentrate on these types of comparisons.

We note that the core sizes used in our numerical comparisons are quite large compared to aircraft vortex cores. Recent laboratory measurements indicate that the cores of our laboratory vortices are much smaller than those used in the numerical simulations. The good agreements presented here between the laboratory experiments and numerical simulations suggest that core size may not be a first-order effect for vortex evolution in a highly stratified environment. We have previously shown that core size is important in numerical simulations for the long-time evolution of vortices in an unstratified environment (unpublished), but is relatively unimportant for very early evolution times. This result implies that core size is an important aspect of vortex evolution, but its effect may only be felt at times later than those in this study.

Finally, it is important to determine the effects of vortex evolution in a realistic environment, including the effects of stratification, turbulence, and shear. An example of the type of question that needs to be addressed is whether the instability observed here would be observed in an environment with ambient turbulence, or whether turbulence effects would dominate this instability. We do not have any answer to this question, but we raise it as a topic for researchers to pursue in the future.

It is generally acknowledged that meandering of the trailing vortex wake can be due to ambient turbulent scales advecting the vortices, although no studies to our knowledge have quantified this effect. The results presented here indicate that a vertical oscillation of up to $0.4b_0$ can be due solely to stratification, even in a nonturbulent environment. Since b_0 for a commercial aircraft can be 50 m, this implies a vertical meandering of 20 m due to stratification effects alone, with horizontal wavelengths around 100 m. Using b_0 for Boeing-737 and 747 aircraft and V_0 based on typical aircraft cruise parameters, for a nondimensional time of 4, this corresponds to distances of ~10–25 km behind the aircraft.

VI. Conclusions

The important conclusions from this study are the following:

1) In an unstratified, nonturbulent, and unsheared fluid, our observations confirm that the primary vortex instability is the Crow instability, as previously predicted by Crow.[2]

2) In an unstratified, nonturbulent, and unsheared fluid, we do not observe large amplitude, short-scale waves (of order b_0) on vortex cores as observed in the laboratory experiments of Thomas and Auerbach[7] and Leweke and Williamson.[6,7] We attribute our lack of these small-scale waves to our larger vortex Reynolds numbers (see Table 3) and to our different vortex generation mechanism (towed wings at an angle of attack compared to generation from the motion of one or more flat plates).

3) In a stratified, nonturbulent, and unsheared fluid, we observe the growth of large amplitude, short-scale waves ($0.5b_0$–$3b_0$) in vortex evolution in highly stratified environments ($Fr \sim 1$). We believe this is the first observation of these short-scale waves from vortex evolution in a stratified flow. For a commercial aircraft, the vertical peak-to-peak amplitude oscillation of the vortex cores due to this instability could be up to 20 m with a horizontal wavelength around 100 m.

Acknowledgments

This study was performed under Contracts N00014-92-C-0231 and N00014-96-C-0060 from the Office of Naval Research. The support and encouragement of L. Patrick Purtell are gratefully acknowledged. Numerical results were computed on computer systems at the U.S. Department of Defense Major Shared Resource Centers CEWES (now known as ERDC) and NAVO. Finally, we acknowledge useful discussions with T. Leweke, T. Sarpkaya, and C. H. K. Williamson and useful comments from P. Bandyopadhyay.

References

[1]Scorer, R. S., "Condensation Trails," *Weather*, Vol. 10, No. 9, 1955, p. 281.

[2]Crow, S. C., "Stability Theory for a Pair of Trailing Vortices," *AIAA Journal*, Vol. 8, No. 12, 1970, pp. 2172–2179.

[3]Sarpkaya, T., "Trailing Vortices in Homogenous and Density-Stratified Media," *Journal of Fluid Mechanics*, Vol. 136, 1983, pp. 85–109.

[4]Robins, R. E., and Delisi, D. P., "Numerical Simulations of Three-Dimensional Trailing Vortex Evolution,"*AIAA Journal*, Vol. 35, No. 9, 1997, pp. 1552–1555.

[5]Thomas, P. J., and Auerbach, D., "The Observation of the Simultaneous Development of a Long- and a Short-Wave Instability Mode on a Vortex Pair," *Journal of Fluid Mechanics*, Vol. 265, 1994, pp. 289–302.

[6]Leweke, T., and Williamson, C. H. K., "The Long and Short of Vortex Pair Instability," *Physics of Fluids*, Vol. 8, No. 9, 1996, p. S5.

[7]Leweke, T., and Williamson, C. H. K., "Cooperative Elliptic Instability of a Vortex Pair," *Journal of Fluid Mechanics*, Vol. 360, 1998, pp. 85–119.

[8]Sarpkaya, T., and Suthon, P., "Interaction of a Vortex Couple with a Free Surface," *Experiments in Fluids*, Vol. 11, No. 4, 1991, pp. 205–217.

[9]Spalart, P. R., "On the Motion of Laminar Wing Wakes in a Stratified Fluid," *Journal of Fluid Mechanics*, Vol. 327, 1996, pp. 139–160.

[10]Robins, R. E., and Delisi, D. P., "Numerical Simulation of Three-Dimensional Trailing Vortex Evolution in Stratified Fluid," *AIAA Journal*, Vol. 36, No. 6, 1998, pp. 981–985.

[11]Fortuin, J. M. H., "Theory and Application of Two Supplementary Methods of Constructing Density Gradient Columns," *Journal of Polymer Science*, Vol. 44, 1960, pp. 505–515.

[12]Delisi, D. P., and Dunkerton, T. J., "Laboratory Observations of Gravity Wave Critical-Layer Flows," *Pure and Applied Geophysics*, Vol. 130, Nos. 2/3, 1989, pp. 445–461.

[13]Lele, S. K., "Compact Finite Difference Schemes with Spectral-Like Resolution," *Journal of Computational Physics*, Vol. 103, 1992, pp. 16–42.

[14]Widnall, S. E., Bliss, D., and Zalay, A., "Theoretical and Experimental Study of the Stability of a Vortex Pair," in *Aircraft Wake Turbulence and Its Detection*, edited by J. Olsen, A. Goldberg, and M. Rogers, Plenum, New York, 1971, pp. 305–338.

[15]Widnall, S. E., "The Structure and Dynamics of Vortex Filaments," *Annual Review of Fluid Mechanics*, Vol. 7, 1975, pp. 141–165.

[16]Widnall, S. E., Bliss, D. B., and Tsai, C.-Y., "The Instability of Short Waves on a Vortex Ring," *Journal of Fluid Mechanics*, Vol. 66, 1974, pp. 35–47.

[17]Tsai, C.-Y., and Widnall, S. E., "The Stability of Short Waves on a Straight Vortex Filament in a Weak Externally Imposed Strain Field," *Journal of Fluid Mechanics*, Vol. 73, Pt. 4, 1976, pp. 721–733.

[18]Billant, P., Brancher, P., and Chomaz, J.-M., "Three-Dimensional Stability of a Vortex Pair," *Physics of Fluids*, Vol. 11, No. 8, 1999, pp. 2069–2077.

[19]Delisi, D. P., Greene, G. C., and Robins, R. E., "Comparison of Laboratory Wake Vortices with Aircraft Vortices," *Annales Geophysicae of the European Geophysical Society*, Vol. 16, Supplement III, 1998, C958.

[20]Hinton, D. A., "An Aircraft Vortex Spacing System (AVOSS) for Dynamical Wake Vortex Spacing Criteria," *AGARD Symposium: The Characterisation and Modification of Wakes from Lifting Vehicles in Fluids*, CP-584, AGARD, Nov. 1996.

P. R. Bandyopadhyay
Associate Editor